

# The clustering of X-ray selected AGN at $z=0.1$

G. Mountrichas, A. Georgakakis

*National Observatory of Athens, V. Paulou & I. Metaxa, 11532, Greece*

21 March 2022

## ABSTRACT

The clustering properties of moderate luminosity ( $L_X = 10^{41} - 10^{44} \text{ erg s}^{-1}$ ) X-ray selected AGN at  $z \approx 0.1$  are explored. X-ray sources in the redshift interval  $0.03 < z < 0.2$  are selected from a serendipitous XMM survey of the SDSS footprint (XMM/SDSS) and are cross-correlated with the SDSS Main galaxy sample. The inferred X-ray AGN auto-correlation function is described by a power law with amplitude  $r_0 \approx 5 h^{-1} \text{ Mpc}$  and slope  $\gamma \approx 2.0$ . The corresponding mass of the dark matter haloes that host X-ray AGN at  $z \approx 0.1$  is  $\approx 10^{13} h^{-1} M_\odot$ . Comparison with studies at higher redshift shows that this mass scale is characteristic of moderate luminosity X-ray AGN out to  $z \approx 1$ . Splitting the AGN sample by rest-frame colour shows that X-ray sources in red hosts are more clustered than those associated with blue galaxies, in agreement with results at  $z \approx 1$ . We also find that the host galaxies of X-ray AGN have lower stellar masses compared to the typical central galaxy of a  $\approx 10^{13} h^{-1} M_\odot$  dark matter halo. AGN hosts either have experienced less stellar mass growth compared to the average central galaxy of a  $\approx 10^{13} h^{-1} M_\odot$  halo or a fraction of them are associated with satellite galaxies.

**Key words:** galaxies: active, galaxies: haloes, galaxies: Seyfert, X-rays: diffuse background

## 1 INTRODUCTION

Observations (e.g. Ferrarese & Merritt 2000, Gebhardt et al. 2000) and theoretical arguments (e.g. Silk 1998, King 2005) suggest that the growth of supermassive black holes (SMBHs) at the centres of galaxies are intimately related to the formation of their hosts. However, the details of the interplay between these two components are still not well understood.

The environment of AGN, i.e. the mass of the typical dark matter halo (DMH) in which they live, is a powerful diagnostic of the physics that drive the formation of SMBHs and their hosts. Different models for the co-evolution of AGN and galaxies make specific testable predictions on how the environment of active SMBHs depends on redshift and accretion luminosity (e.g. Marulli et al. 2006, Hopkins et al. 2007, Fanidakis 2010, Degraf et al. 2010, Bonoli et al. 2009). Moreover, there has been progress recently in phenomenological methods to associate baryons to DMHs at different redshifts, to infer in a least model dependent way how galaxies evolve at different environments (e.g. Zheng et al. 2007, Conroy & Wechsler 2009, Zehavi et al. 2011, Avila-Reese & Firmani 2011). By determining the typical DMH of AGN one can place them in the context of those studies to explore the conditions under which SMBH grow at different epochs.

An advantage of studying the environment of AGN is that it provides one of the few diagnostics of the AGN/galaxy interplay that is immune to contamination of the stellar light of galaxies by emission from the central engine. AGN can easily outshine their hosts, thereby rendering studies of the stellar mass, star-formation history and morphology of their hosts challenging and prone to systematics. This poses a serious limitation in the comparison between observations and models for the growth of SMBHs and highlights the importance of clustering studies.

Powerful UV bright QSOs are one of the few AGN classes for which tight constraints on their large scale distribution are available. This is because of the apparent brightness of these sources in the optical which has allowed large spectroscopic follow-up programs, such as the 2QZ (2dF QSO Redshift Survey, Croom et al. 2004), SDSS (Sloan Digital Sky Survey, Richards et al. 2002, Schneider et al. 2005) and 2SLAQ (2dF-SDSS LRG and QSO Survey, Cannon et al. 2006, Croom et al. 2008). The picture emerging from those studies is that powerful UV bright QSOs live in dark matter haloes of few times  $10^{12} h^{-1} M_\odot$  almost independent of redshift and accretion luminosity (e.g. Croom et al. 2005, Myers et al. 2007, da Ángela et al. 2008, Ross et al. 2009, Ivashchenko et al. 2010, but see Mountrichas et al. 2009). These properties are broadly consistent with the predictions

of the merger model for the growth of SMBH (e.g. Hopkins et al. 2007, Bonoli et al. 2009), suggesting that powerful QSOs are the product of interactions between gas rich galaxies.

The QSOs selected in the above surveys however, represent luminous and rare sources above the knee of the AGN luminosity function. Therefore, they are not representative of the overall AGN population and their contribution to the accretion power of the Universe is small. Additionally, their selection at UV/optical wavelengths raises concerns on possible biases against obscured sources. Observations at X-ray wavelengths provide an efficient way of selecting AGN over a wide luminosity baseline nearly independent of obscuration. Study of the clustering of X-ray AGN can therefore constrain the fueling mechanism of the sources that dominate the accretion history of the Universe. Despite considerable progress in the last few years however, the large scale distribution of X-ray AGN is still not well constrained. This is primarily because of the apparent faintness of these sources at optical wavelengths and their relatively high surface density on the sky, which make large spectroscopic follow-up programs, similar to those carried out for UV bright QSOs, extremely expensive in telescope time.

In the absence of any follow-up observations, the most widely used approach for studying the clustering of X-ray AGN is the angular auto-correlation function (e.g. Basilakos et al. 2004, 2005, Plionis et al. 2008, Ebrero et al. 2009). The main limitation of this approach is that assumptions have to be made on the redshift distribution of the AGN population to infer the mass of their dark matter haloes. This introduces systematics and model dependent biases which can be large. This problem has been mitigated by extensive follow-up spectroscopic programs in selected few X-ray survey fields (e.g. Barger et al. 2003, Brusa et al. 2009), which allowed estimation of the real-space auto-correlation function of X-ray AGN samples (e.g. Mullis et al. 2004, Gilli et al. 2005, 2009, Yang et al. 2006, Allevato et al. 2011). One of the results from these studies is the importance of sample variance. Spikes in the redshift distribution of X-ray sources can significantly affect clustering studies in current X-ray surveys, which typically have small angular sizes (e.g. Gilli et al. 2005, 2009). An alternative approach for studying the large scale distribution of AGN is the real-space cross-correlation function with galaxies over the same cosmological volume (e.g. Coil et al. 2009, Krumpel et al. 2010). This approach has certain merits compared to auto-correlation function methods, as long as the clustering of the galaxy population is known to a good level of accuracy and spectroscopy is available for the AGN. Firstly, the space density of galaxies is typically much larger than that of AGN, thereby suppressing random errors when counting AGN/galaxy pairs. Secondly, by cross-correlating AGN with galaxies in the same field the impact of sample variance is minimised. The studies above suggest that X-ray AGN live in dark matter haloes with masses  $5 \times 10^{12} - 5 \times 10^{13} h^{-1} M_{\odot}$ , which are, on average, more massive than those of UV bright QSOs. The wide range in the estimated DMH masses could be the result of random errors and systematics that affect individual measurements or because the AGN clustering may depend on the accretion luminosity, the redshift and/or the level of obscuration of the central engine (e.g. Plionis 2008, Hickox et al. 2011, Allevato et al. 2011).

In this paper we explore changes in the large scale dis-

tribution of moderate luminosity ( $L_X < 10^{44} \text{ erg s}^{-1}$ ) X-ray selected AGN from  $z \approx 1$  to  $z \approx 0.1$ . We use a serendipitous XMM survey of the SDSS area (XMM/SDSS, Georgakakis & Nandra 2011) to compile a sample of low redshift AGN,  $z \approx 0.1$ . These sources are then cross-correlated with the SDSS Main Galaxy sample (Strauss et al. 2002) to infer their clustering properties. The advantage of the serendipitous XMM/SDSS survey is that the AGN selection function at low redshift is almost identical to that of X-ray AGN at  $z \approx 1$  detected in deep Chandra and XMM surveys. Therefore differential selection effects between low and high redshift samples are minimal. This allows direct comparison of the environment of moderate luminosity X-ray AGN across redshift to investigate possible evolutionary trends. Throughout this paper we adopt  $H_0 = 100 \text{ km s}^{-1} \text{ Mpc}^{-1}$ ,  $\Omega_M = 0.3$  and  $\Omega_{\Lambda} = 0.7$ . Rest frame quantities (e.g. luminosities, dark matter halo masses) are parametrised by  $h = H_0/100$ .

## 2 THE X-RAY AGN SAMPLE

The clustering properties of X-ray AGN at  $z \approx 0.1$  are investigated by selecting low redshift sources detected in a serendipitous XMM survey of the SDSS footprint (XMM/SDSS). The construction of the XMM/SDSS source catalogue, including X-ray source detection, flux estimation and optical identification, is described in Georgakakis & Nandra (2011).

The XMM/SDSS survey includes pointings targeting clusters of galaxies. The overdensity of sources in those fields may bias large scale structure studies. Therefore XMM/SDSS survey fields that have clusters as their prime targets are excluded from the analysis. These observations are identified from the target name keyword of the event files. This reduces the total XMM/SDSS survey area to  $102 \text{ deg}^2$ .

The low redshift X-ray subsample of the XMM/SDSS survey consists of 175 serendipitous hard-band (2-8 keV) and 297 full-band (0.5-8 keV) detections with  $0.03 < z < 0.2$ , X-ray luminosity  $L_X(2 - 10 \text{ keV}) > 10^{41} \text{ erg s}^{-1}$  (see below) and  $r < 17.77 \text{ mag}$  after correcting for Galactic extinction (Schlegel et al. 1998). The magnitude cut corresponds to the limit of the SDSS Main Galaxy Sample (Strauss et al. 2002), which provides the majority of redshifts in the SDSS. The photometry is from the New York University Value-Added Galaxy Catalog (NYU-VAGC, Blanton et al. 2005) which corresponds to the SDSS DR7 (Abazajian et al. 2009). The X-ray luminosity cut is to limit the sample to AGN which contribute substantially to the X-ray luminosity density of the Universe at low redshift (e.g. Aird et al. 2010). As discussed by Georgakakis et al. (2011) contamination by normal galaxies is not a concern for luminosities  $L_X(2 - 10 \text{ keV}) > 10^{41} \text{ erg s}^{-1}$ .

Clustering results are presented for both the full and the hard-band selected AGN samples. The former has the advantage of larger size, thereby improving the statistical reliability of the results. The latter is selected at rest-frame energies of about 2-9 keV at  $z = 0.1$ , which are similar to those of Chandra and XMM X-ray AGN samples at  $z \approx 1$  (typically 1-14 keV). This facilitates the comparison across redshift by minimising differential selection effects.

X-ray luminosities are estimated in the 2-10 keV band after correcting the observed flux in the 2-8 keV band (hard-band selected sample) or the 0.5-8 keV band (full-band selected sample) for intrinsic absorption parametrised by the hydrogen column density,  $N_H$ . For individual X-ray AGN this quantity is determined from the hardness ratios between the soft (0.5-2 keV) and the hard (2-8 keV) X-ray bands assuming an intrinsic power-law X-ray spectrum with index  $\Gamma = 1.9$  (Nandra et al. 1994).

### 3 METHODOLOGY

#### 3.1 AGN clustering estimation

Because the low redshift subset ( $0.03 < z < 0.2$  and  $r < 17.77$  mag) of the XMM/SDSS survey source catalogue is small, we choose to quantify their clustering properties by estimating their cross-correlation function with the much larger sample of SDSS spectroscopically identified galaxies. We use the NYU-VAGC to select a total of 592,017 sources in the SDSS Main Galaxy spectroscopic sample (bit-mask parameter VAG\_SELECT equals 7) with redshifts in the interval  $0.03 - 0.2$  and extinction corrected magnitudes  $r < 17.77$  mag.

Incompleteness in the galaxy redshift catalogue because of fiber collisions is a source of bias in clustering studies. The SDSS fibers have finite size and cannot be placed closer than 55 arcsec, which corresponds to about  $70 h^{-1}$  kpc at  $z = 0.1$ . This separation is too small to affect our results and conclusions as the X-ray/galaxy cross-correlation signal is dominated by pairs on much larger scales (see Results section). We nevertheless correct for this effect by assigning a source that was not observed because of fiber collisions the redshift of the galaxy with which it collided, as proposed by Blanton et al. (2005).

The determination of the cross-correlation function with a large sample of galaxies is superior to the estimation of the auto-correlation function in the case of small samples, like X-ray AGN, because random errors are significantly suppressed. An additional advantage is that the cross-correlation requires knowledge of the selection function of galaxies only, which is less complex than that of X-ray AGN. Also, sample variance is affecting in the same way X-ray AGN and galaxies. The impact of this bias is therefore minimised in the cross-correlation function calculation. The cross-correlation approach however, requires an accurate estimate of the auto-correlation function of galaxies to infer the clustering properties of AGN.

Next we present the equations used to determine the clustering of AGN. Since both the auto-correlation and the cross-correlation functions are special cases of the 2-point statistics of the AGN and galaxy populations, they are both defined by the same basic equations. In this section the term correlation function refers to either the auto-correlation or the cross-correlation functions. When necessary we will differentiate between the two quantities.

The real space correlation function,  $\xi$ , is calculated as

$$\xi = \frac{N_{rd}}{N_{gal}} \frac{DD}{DR} - 1, \quad (1)$$

where  $N_{rd}$  is the number of random points,  $N_{gal}$  is the number of galaxies,  $DD$  are the data-data pairs at separation

$r$ , i.e. AGN-galaxy pairs in the cross-correlation function or galaxy-galaxy pairs in the case of the auto-correlation function,  $DR$  are the AGN-random pairs (cross-correlation) or galaxy-random pairs (galaxy auto-correlation function) at separation  $r$ . Random points within the surveyed area are produced by randomising the positions of SDSS galaxies taking into account the SDSS window function and the spectroscopic completeness of the galaxy sample. The random catalogues provided as part of the NYU-VAGC data release version 7.2 are used. They contain  $\approx 3 \times$  more randoms than galaxies. The random points are distributed with constant surface density in the SDSS footprint as defined by the Large Scale Structure mask of NYU-VAGC (Blanton et al. 2005). The redshifts assigned to the randoms points follow the redshift distribution of the galaxy sample.

When the correlation function is measured in redshift-space, the clustering is affected at small scales by the rms velocity dispersion of AGN along the line of sight and by dynamical infall of matter into higher density regions. If  $s_1$  and  $s_2$  are the distances of two objects 1, 2, measured in redshift-space, and  $\theta$  the angular separation between them, then  $\sigma$  and  $\pi$  are defined as

$$\pi = (s_2 - s_1), \text{ along the line-of-sight,} \quad (2)$$

$$\sigma = \frac{(s_2 + s_1)}{2} \theta, \text{ across the line-of-sight.} \quad (3)$$

These are small angle approximations. Equation 1 then becomes:

$$\xi(\sigma, \pi) = \frac{N_{rd}}{N_{gal}} \frac{DD(\sigma, \pi)}{DR(\sigma, \pi)} - 1, \quad (4)$$

To the first order, the non-linear redshift-space distortions, i.e. the small-scale peculiar velocities, appear only in the radial component. These effects are therefore minimised by integrating  $\xi$  along the  $\pi$  direction. The resulting two-point statistic is the projected correlation function

$$w_p(\sigma) = 2 \int_0^\infty \xi(\sigma, \pi) d\pi. \quad (5)$$

In practice the maximum scale of the integration is set to  $\pi_{max} = 70 h^{-1}$  Mpc (da Ángela et al. 2008). If larger scales are included, the signal will be dominated by noise. If the integration is limited on small scales the amplitude will be underestimated.

In the estimation of the projected AGN/galaxy cross-correlation function each AGN is weighted by the factor  $1/V_{max}$ , the inverse of the maximum volume within which a source can be detected. This accounts for the complex selection function of the XMM/SDSS AGN. Because of vignetting and the spatially varying width of the XMM's Point Spread Function (PSF) the solid angle within which the surveyed area is sensitive to X-ray faint sources is smaller than for brighter ones. As a result lower luminosity AGN are underrepresented in the low redshift subset of the XMM/SDSS survey, but in a way that can be accurately quantified and corrected for in the  $V_{max}$  calculation. It is emphasised that this is a second order correction and does not have a strong impact on the results and conclusions. For simplicity this weight is not included in the equations presented in this section.

Under the assumption that the real-space correlation function follows a power-law of the form  $\xi(r) = \left(\frac{r}{r_0}\right)^{-\gamma}$ ,

the real-space correlation length,  $r_0$ , and slope,  $\gamma$ , can be estimated directly from the projected correlation function

$$\frac{w_p(\sigma)}{\sigma} = \left(\frac{r_0}{\sigma}\right)^\gamma \frac{\Gamma(\frac{1}{2})\Gamma(\frac{\gamma-1}{2})}{\Gamma(\frac{\gamma}{2})}, \quad (6)$$

where  $\Gamma(x)$  is the Gamma function. This is because equation 5 can be rewritten as

$$w_p(\sigma) = 2 \int_{\sigma}^{\pi^{max}} \frac{r\xi(r)}{\sqrt{r^2 - \sigma^2}} dr, \quad (7)$$

and then solved analytically by substituting the power-law form for  $\xi(r)$ .

The projected correlation function can also be used to estimate the real-space correlation function,  $\xi(r)$ , even if a power law form is not adopted. By inverting  $w_p(\sigma)$  (Saunders et al. 1992)

$$\xi(r) = -\frac{1}{\pi} \int_r^{\infty} \frac{d w(\sigma)/d\sigma}{\sqrt{(\sigma^2 - r^2)}} d\sigma \quad (8)$$

and assuming a step function for  $w_p(\sigma) = w_i$  it is found

$$\xi(\sigma_i) = -\frac{1}{\pi} \sum_{j \geq i} \frac{\omega_{j+1} - \omega_j}{\sigma_{j+1} - \sigma_j} \ln\left(\frac{\sigma_{j+1} + \sqrt{\sigma_{j+1}^2 - \sigma_i^2}}{\sigma_j + \sqrt{\sigma_j^2 - \sigma_i^2}}\right) \quad (9)$$

for  $r = \sigma_i$ . That measurement is generally more noisy than  $w_p(\sigma)$ . The projected correlation function and equation 6 are therefore used to infer  $r_0$  and  $\gamma$ , under the assumption of power-law for  $\xi$ . However, we check that the  $r_0$  and  $\gamma$  values obtained by equation 6 provide a good approximation to the real-space correlation function inferred from equation 9.

The above procedure allows us to measure the AGN-galaxy projected cross-correlation function,  $w_p(AG)$ , and the galaxy projected auto-correlation function,  $w_p(GG)$ . Using these measurements and assuming a linear bias, the AGN projected auto-correlation function,  $w_p(AA)$ , is

$$w_p(AA) = \frac{w_p(AG)^2}{w_p(GG)}. \quad (10)$$

For the estimation of errors of the correlation function measurements the survey area is split into six subregions, each of which includes nearly equal number of X-ray AGN. The cross-correlation function is then estimated for each of the six subregions. The variance at a given scale is

$$\sigma^2 = \frac{1}{N-1} \sum_{L=1}^N \frac{DR_L}{DR} [\xi_L - \xi]^2, \quad (11)$$

where  $N$  is the number of fields, i.e.  $N=6$ ,  $DR_L$  is the AGN-random pairs in the field,  $DR$  is the overall number of AGN-random pairs,  $\xi_L$  is the correlation function measured in a subregion and  $\xi$  is the overall correlation function.

### 3.2 Estimation of the bias parameter

The bias parameter of AGN relative to the underlying dark matter halo distribution is estimated using two different approaches that are often adopted in the literature. This is to facilitate direct comparison of our results with previous studies.

The first method uses the integrated projected AGN/galaxy cross-correlation function and normalizes the result to the volume contained in a sphere with radius of

$20h^{-1}$  Mpc (e.g. Ross et al. 2009, Mountrichas et al. 2009, da Ângela et al. 2008)

$$\xi_{20} = \frac{3}{20^3} \int_{r_{min}}^{r_{max}} \xi(r) r^2 dr. \quad (12)$$

where  $\xi_{20}$  is the integrated cross-correlation function. The lower and upper limits are set to 1 and  $20h^{-1}$  Mpc, respectively. For the estimation of  $\xi_{20}$ , our  $w_p(\sigma)$  measurements are used. The galaxy bias,  $b_G$ , is estimated as

$$b_G^2 = \frac{\xi_{GG}}{\xi_{mm}} \Rightarrow b_G \approx \sqrt{\frac{\xi_{20}^{GG}}{\xi_{20}^{mm}}}, \quad (13)$$

where  $\xi_{20}^{mm}$  is the integrated correlation function of dark matter. It is estimated from the normalized  $\Lambda$ CDM power spectrum model of Smith et al. (2003) for cosmological parameters  $\Omega_m(z=0) = 0.3$ ,  $\Omega_\Lambda(z=0) = 0.7$ ,  $\Gamma = 0.17$  and  $\sigma_8 = 0.8$ , in accordance with the recent WMAP results (Spergel et al. 2007). The value of  $\sigma_8$  has been revised by the latest analysis of the WMAP data from 0.84 to 0.8. To facilitate the comparison with previous studies we also present results for  $\sigma_8 = 0.84$ .

Having measured the galaxy bias we can then estimate the AGN bias,  $b_A$ , from the relation

$$b_A b_G = \frac{\xi_{AG}}{\xi_{mm}} \Rightarrow b_A \approx \frac{1}{b_G} \frac{\xi_{20}^{AG}}{\xi_{20}^{mm}}, \quad (14)$$

where  $\xi_{20}^{AG}$  is the integrated AGN/galaxy cross-correlation function. The equation above also assumes scale independent bias.

The second approach for estimating the bias uses the best-fit  $r_0$  and  $\gamma$  values of the inferred AGN auto-correlation function, obtained from equation 10 (e.g. Krumpel et al. 2010). The clustering strength is expressed in terms of the rms fluctuation of the density distribution over a sphere with a comoving radius of  $8h^{-1}$  Mpc

$$\sigma_{8,AGN}^2 = J_2(\gamma) \left(\frac{r_0}{8h^{-1} \text{Mpc}}\right)^\gamma, \quad (15)$$

where

$$J_2(\gamma) = \frac{72}{(3-\gamma)(4-\gamma)(6-\gamma)2^\gamma}, \quad (16)$$

the AGN bias can be calculated via

$$b_{AGN} = \frac{\sigma_{8,AGN}}{\sigma_8(z)}. \quad (17)$$

The bias of AGN or galaxies is related to the mass of the dark matter halos they live in (e.g. Mo & White 1996). Therefore their clustering properties can be used to infer their dark matter halo masses. In this calculation the ellipsoidal collapse model of Sheth, Mo & Tormen (2001) is adopted. The methodology described by da Ângela et al. (2008) and van den Bosch (2002) is followed to convert the bias measurements to dark matter halo masses. We use the bias values estimated from the  $\sigma_{8,AGN}$  rms fluctuation of the density distribution.

## 4 RESULTS

Figure 1 (left panel) compares the full-band AGN-galaxy cross-correlation function,  $w_p(AG)$ , with the galaxy auto-correlation function,  $w_p(GG)$ . Galaxies are less clustered

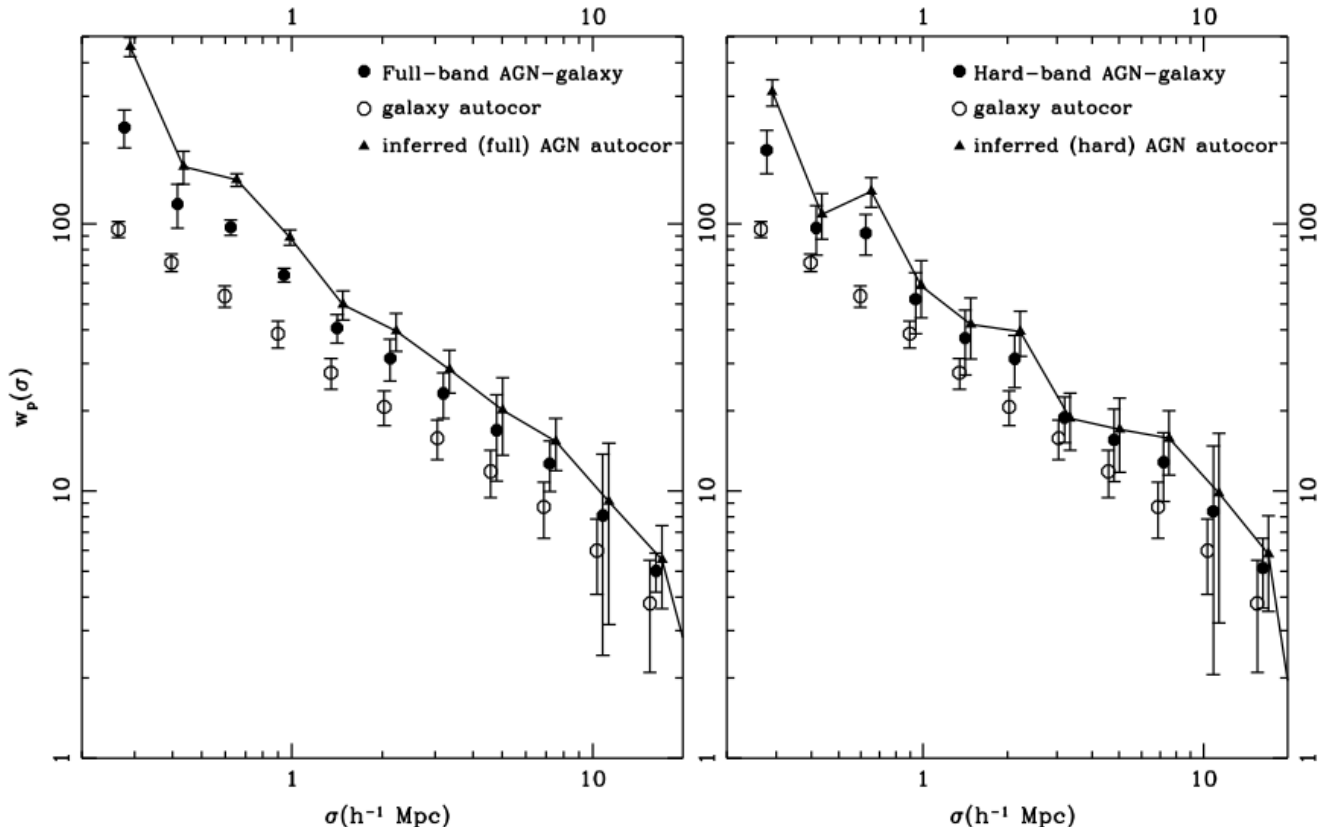


**Figure 1.** Left panel: The full-band AGN-galaxy cross-correlation is shown by filled circles. Open circles show the galaxy auto-correlation results. Solid triangles connected with the solid line show the inferred full-band AGN auto-correlation function. Right panel: Same as in the left panel but using the hard-band AGN sample. For clarity, open circles and solid triangles are offset in the horizontal direction by  $\delta \log \sigma = -0.02$  and  $+0.02$ , respectively.

than AGN at all scales. The inferred AGN projected auto-correlation function,  $w_p(AA)$ , (i.e. equation 10) is also plotted in the figure. The errors in  $w_p(AA)$  are estimated by adding in quadrature the uncertainties of  $w_p(AG)$  and  $w_p(GG)$ . The right panel of Figure 1 shows the clustering results for the hard-band AGN sample. Within the errors the clustering of those sources is similar to the full-band sample. This is also shown in Tables 1 and 2, which present the best-fit estimates for the  $r_0$  and  $\gamma$  for the cross-correlation and the auto-correlation functions respectively, assuming a power-law form for  $\xi$ . Scales in the interval  $0.25 - 17 h^{-1} \text{Mpc}$  are used to fit the data. The errors correspond to the 68th percentile around the minimum  $\chi^2$ .

The assumption that the real-space correlation function is well approximated by a power law is justified by Figure 3. It compares the inferred  $\xi(r)$  for the AGN/galaxy cross-correlation and the galaxy auto-correlation function without making any assumptions on its functional form (i.e. equations 8, 9) with power-law fits using the  $r_0$  and  $\gamma$  values of Tables 1 and 2.

We can therefore use the best-fit parameters for  $r_0$  and  $\gamma$  to estimate the bias of AGN and galaxies (equations 12–17). The results are presented in Table 3, where  $b(\xi_{20})$  and  $b(\sigma_8)$  are respectively the biases estimated from the first and the second method described in section 3.2. The errors are deter-

mined from the variance across the six subregions of the surveyed area. Within the uncertainties the bias values, calculated from the two different methods are consistent. We caution that the  $b(\sigma_8)$  and  $b(\xi_{20})$  are determined from slightly different scales. The former is based on the  $r_0$  and  $\gamma$  parameters estimated by fitting the projected cross-correlation function on scales of  $0.25 - 17 h^{-1} \text{Mpc}$ . The latter is determined by integrating the  $\xi(r)$  from  $1.0$  to  $20 h^{-1} \text{Mpc}$ . We have confirmed however, that this difference does not change the results and conclusions.

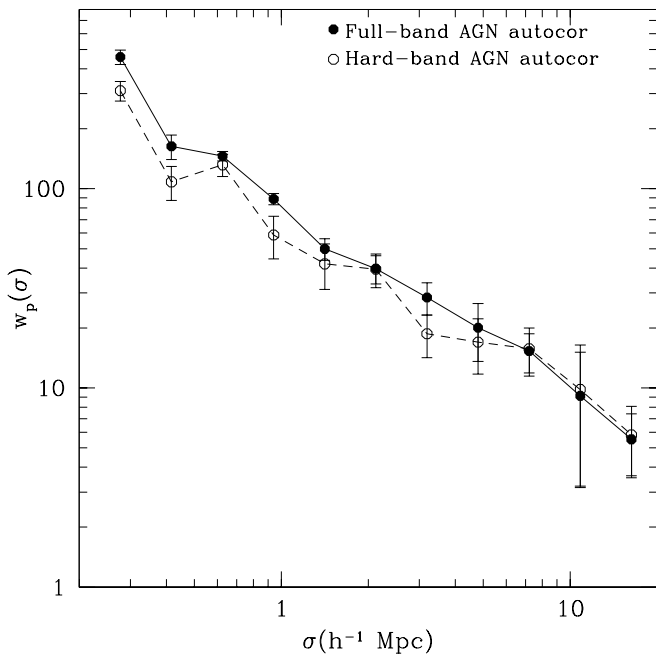
Next, we explore variations in the clustering of X-ray AGN with rest-frame optical colour. This is motivated by previous studies suggesting that AGN in red cloud hosts are more clustered than those in blue cloud galaxies (e.g. Coil et al. 2009). For this exercise we use the full-band AGN sample because of its larger size. Red/blue galaxies/AGN are separated by their  $^{0.1}(u-g)$  rest-frame colour, i.e. the difference between the absolute magnitudes of the source in the  $^{0.1}u$ ,  $^{0.1}g$  bands, which are the SDSS  $u$ ,  $g$  filters shifted to  $z = 0.1$ . The calculation of  $^{0.1}(u-g)$  is carried out using the KCORRECT version 4.2 routines (Blanton & Roweis 2007). The distribution of X-ray AGN and galaxies in  $^{0.1}(u-g)$  colour is plotted in Figure 4. The division between red and blue galaxies and AGN is set to  $^{0.1}(u-g) = 1.5$  (Blanton 2006). There are 325,510 galaxies and 154 X-ray AGN with

**Table 1.**  $r_0$  and  $\gamma$  values for  $\xi(r)$  (scales of  $0.25 - 17h^{-1}\text{Mpc}$ ) for the cross-correlation measurements.

|          | AGN (full )            | Red AGN         | Blue AGN        | AGN (Hard)      | Red galaxies    | Blue galaxies   |
|----------|------------------------|-----------------|-----------------|-----------------|-----------------|-----------------|
| $r_0$    | $4.4^{+0.1}_{-0.2}$    | $4.9 \pm 0.4$   | $4.1 \pm 0.2$   | $4.3 \pm 0.2$   | $4.80 \pm 0.06$ | $3.60 \pm 0.05$ |
| $\gamma$ | $2.00^{+0.06}_{-0.09}$ | $1.98 \pm 0.10$ | $1.95 \pm 0.05$ | $1.90 \pm 0.11$ | $1.82 \pm 0.01$ | $1.71 \pm 0.01$ |

**Table 2.**  $r_0$  and  $\gamma$  values for  $\xi(r)$  (scales of  $0.25 - 17h^{-1}\text{Mpc}$ ) for the galaxy auto-correlation and for the inferred auto-correlation function using equation 10.

|          | AGN (full )     | Red AGN         | Blue AGN        | AGN (Hard)      | galaxies        | Red galaxies    | Blue galaxies   |
|----------|-----------------|-----------------|-----------------|-----------------|-----------------|-----------------|-----------------|
| $r_0$    | $5.0 \pm 0.5$   | $6.6 \pm 0.6$   | $4.7 \pm 0.4$   | $4.8 \pm 0.6$   | $4.00 \pm 0.05$ | $5.00 \pm 0.10$ | $2.90 \pm 0.05$ |
| $\gamma$ | $2.00 \pm 0.11$ | $1.82 \pm 0.19$ | $2.12 \pm 0.16$ | $2.02 \pm 0.18$ | $1.76 \pm 0.01$ | $1.90 \pm 0.02$ | $1.58 \pm 0.01$ |

**Figure 2.** Filled circles show the inferred full-band AGN auto-correlation and open circles the inferred hard-band AGN auto-correlation. For clarity, open and filled circles are offset in the horizontal direction by  $\delta \log \sigma = -0.01$  and  $+0.01$ , respectively.

colours bluer than that cut (blue subsamples) and 266,508 galaxies and 143 X-ray AGN with  $^{0.1}(u-g) > 1.5$  (red subsamples).

Figure 5 plots the projected cross-correlation of red and blue galaxies with the full galaxy sample. The relevant  $r_0$  and  $\gamma$  best-fit values, bias parameters and dark matter halo masses are shown in Tables 2 and 3. As expected red galaxies are more clustered than blue ones at all scales, in agreement with previous studies (e.g. Madgwick et al. 2003, Zehavi et al. 2005, Coil et al. 2008, Hickox et al. 2009). The projected cross-correlation function of red/blue AGN with the overall galaxy population is shown in Figure 6. The clustering results are presented in Tables 2 and 3. X-ray AGN follow the

same pattern with galaxies, i.e. active SMBH in red hosts are more clustered than those in blue galaxies.

This is further demonstrated in Table 4 which presents the relative bias of different subsamples, defined as the ratio between the  $w_p(\sigma)$  measurements of the subsample,  $b_{rel} = \sqrt{w_p(\sigma)_1/w_p(\sigma)_2}$  (Coil et al. 2007), integrated over two scales,  $0.25 - 8h^{-1}\text{Mpc}$  and  $1 - 8h^{-1}\text{Mpc}$ . The errors on these measurements are estimated from the variance of the relative bias across the six subregions of the survey area (Section 3.1). This table confirms that red AGN and galaxies cluster more than blue AGN and galaxies, respectively. Also, the overall X-ray AGN population has similar clustering properties as red galaxies but is more clustered than blue ones.

We also investigate the dependence of the clustering on luminosity and X-ray obscuration by splitting the sample into two nearly equal size groups at  $\log L_X = 41.8$  (erg/s) and  $\log N_H = 22$  ( $\text{cm}^{-2}$ ) respectively. We do not find any statistically significant trends of the AGN clustering with luminosity or X-ray hardness. This null result maybe be because of the relatively narrow luminosity and obscuration baselines of our low redshift X-ray AGN sample. Cappelluti et al. (2010) for example, find a higher clustering for type I AGN compared to type IIs. Their sample is drawn from the SWIFT-BAT AGN catalogue, which is sensitive to heavily obscured systems. Also, Krumpe et al. (2010) find evidence for higher clustering only for very bright AGN,  $L_X > 10^{44}$  ergs $^{-1}$ . The low redshift subset of the XMM/SDSS survey does not have the volume to detect such powerful sources.

Finally, we calculate the masses of the dark matter halos that host AGN and galaxies, as described in Section 3.2. The results appear in Table 3. We do not estimate a lower limit for the mass of the halos that host blue galaxies. This is because the  $1\sigma$  lower limit of the bias of those sources is  $b = 0.69$  and the minimum bias value derived from Sheth et al. (2001) is  $b = 0.72$ . The calculations show that moderate luminosity AGN at  $z \approx 0.1$  reside in dark matter halos with typical mass  $M_{DMH} \approx 10^{13} h^{-1} M_\odot$ .

The AGN bias and DMH mass estimates presented in Table 3 are robust to the details of the adopted methodology. Cosmic variance is a concern as in the cross-correlation function estimation we use all SDSS galaxies, not just those

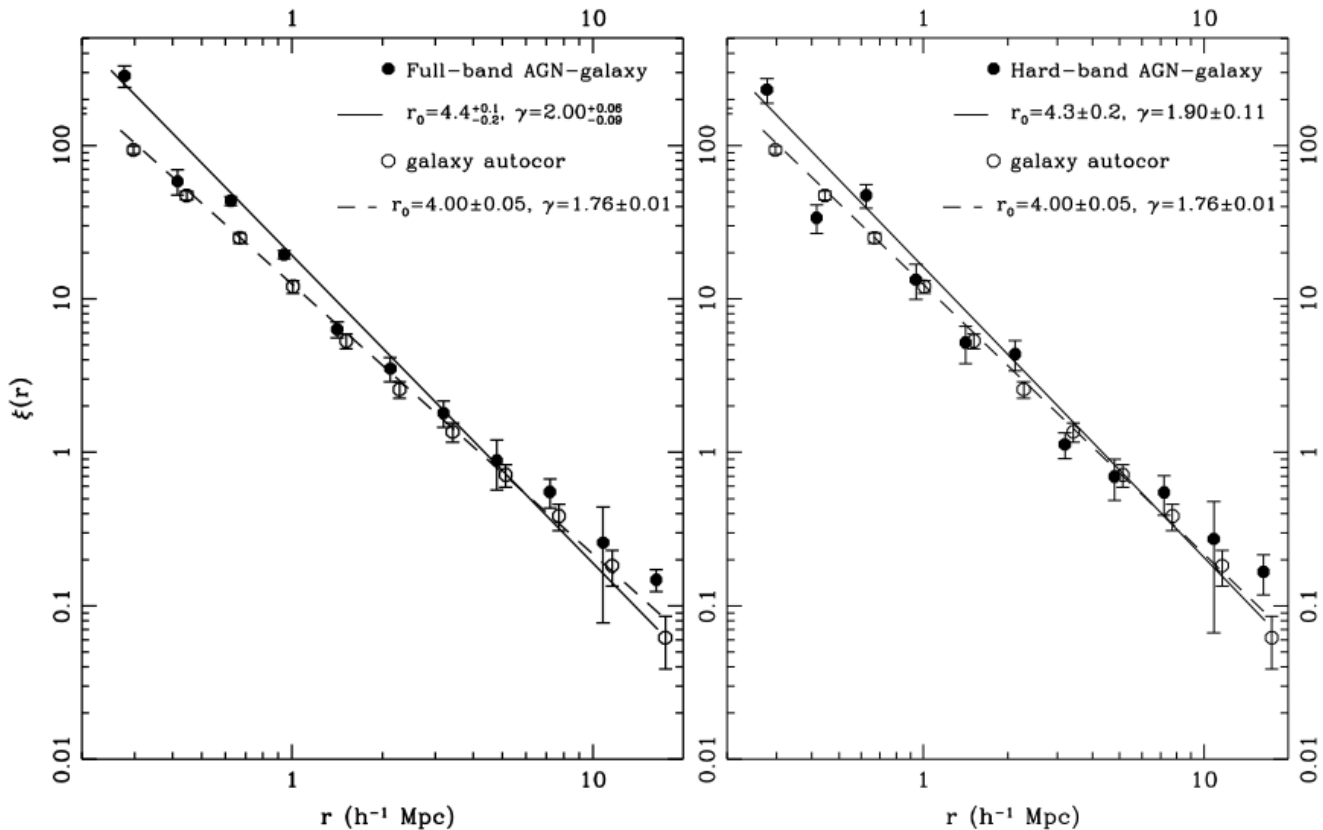


**Figure 3.** Left panel: The full-band AGN-galaxy cross-correlation function in real-space is shown by filled circles. The solid line shows the fit on scales  $0.25 < r < 17 h^{-1} \text{Mpc}$ . Open circles show the galaxy auto-correlation results and the fit is shown by the dashed line. Right panel: Same as in the left panel but using the hard-band AGN sample. For clarity, open circles are offset in the horizontal direction by  $\delta \log \sigma = +0.03$ .

overlapping with the XMM pointings. Therefore the cosmological volumes of the AGN and galaxy samples are different. We repeat the analysis for the full-band selected AGN sample using only those SDSS galaxies that lie within the XMM fields of our serendipitous survey. This exercise yields the same AGN bias as in Table 3. Additionally, the exclusion of XMM pointings targeting clusters (see section 2) might appear arbitrary and subjective. We include AGN in those fields and cross-correlate them with the SDSS galaxies in the same cosmological volume, i.e. those overlapping with the XMM pointings of the XMM/SDSS survey. The inferred full-band AGN bias is 10 per cent lower compared to that listed in Table 3, i.e. within the estimated errors.

## 5 COMPARISON WITH PREVIOUS STUDIES

In this section our bias estimates for X-ray AGN at  $z \approx 0.1$  are compared with previous studies that select active SMBH either at X-rays or UV/optical. To facilitate the direct comparison and present the results from different papers in a uniform manner we re-estimate the bias from each study using the quoted  $r_0$  and  $\gamma$  values based on the  $\sigma_8$  methodology of section 3.1. Studies that have measured only the redshift-space correlation function and do not provide real-space  $r_0$  and  $\gamma$  values are excluded from the analysis. Moreover, an-

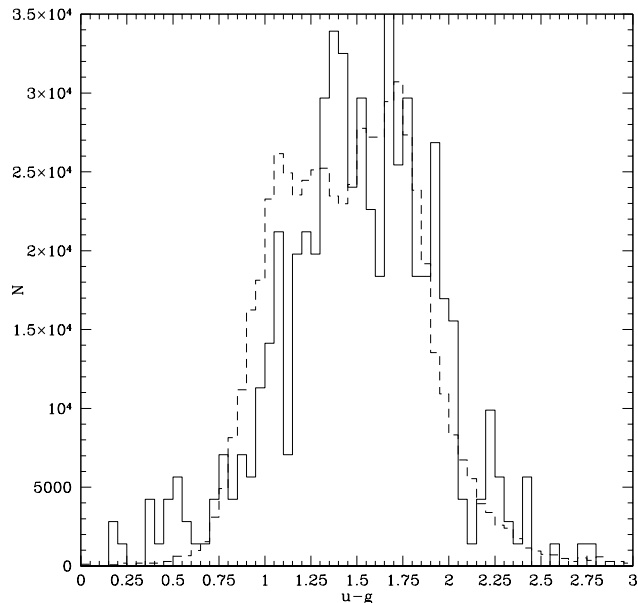
gular auto-correlation function studies are not included in our compilation as the deprojection of the angular signal to 3-dimensions using the Limber's formula (Limber 1953) may introduce systematic uncertainties.

Table 5 presents the studies used for these measurements and the most important properties of the samples they used. The errors on  $b(\sigma_8)$  are calculated based on the errors on  $r_0$ ,  $\gamma$ . The bias parameter is compared with our measurement in Figure 7 and the expected evolution of the bias for different dark matter halo masses. Below we comment on selected datapoints appearing in Table 5.

From the high redshift samples plotted in Figure 7 the Coil et al. (2009) datapoint is the most appropriate to compare with our measurement of the bias at  $z \approx 0.1$ . They select X-ray AGN at  $z \approx 1$  at rest-frame energies of about 1-14 keV similar to those used here. The luminosity range of their AGN is similar to our low redshift sample. They also use the cross-correlation function with galaxies to improve on the statistics and minimise sample variance effects in their calculations. The mass of the dark matter halos that host these high redshift X-ray AGN, as estimated based on the quoted  $r_0$  and  $\gamma$  values by Coil et al. (2009), is in good agreement with our measurements at low redshift. This shows that moderate luminosity X-ray AGN live in dark matter haloes of similar mass,  $\sim 10^{13} h^{-1} M_\odot$ , at all redshifts out to  $z \approx 1$ .

**Table 3.** Bias values for AGN and galaxy samples using the two approaches discussed in the text. Values marked with \* are calculated for  $\sigma_8 = 0.84$ . The  $\xi_{20}$  values are from the cross-correlation measurements (except for galaxies). The  $M_{DMH}$  are based on  $b(\sigma_8 = 0.8)$ .

|  | AGN (full)              | Red AGN                 | Blue AGN                | AGN (hard)              | galaxies                | Red galaxies            | Blue galaxies          |
|--|-------------------------|-------------------------|-------------------------|-------------------------|-------------------------|-------------------------|------------------------|
| $\xi_{20}$   | $0.22^{+0.03}_{-0.05}$  | $0.26^{+0.02}_{-0.05}$  | $0.18^{+0.04}_{-0.03}$  | $0.21^{+0.03}_{-0.03}$  | $0.17^{+0.02}_{-0.01}$  | $0.23^{+0.03}_{-0.02}$  | $0.15^{+0.01}_{-0.01}$ |
| $\sigma_{8,AGN}$                                   | $0.94 \pm 0.10$         | $1.16 \pm 0.16$         | $0.92 \pm 0.11$         | $0.91 \pm 0.13$         | $0.73 \pm 0.01$         | $0.91 \pm 0.01$         | $0.57 \pm 0.01$        |
| $b(\xi_{20})$                                      | $1.30^{+0.20}_{-0.27}$  | $1.52^{+0.17}_{-0.28}$  | $1.07^{+0.24}_{-0.17}$  | $1.25^{+0.20}_{-0.12}$  | $0.93^{+0.05}_{-0.03}$  | $1.37^{+0.20}_{-0.12}$  | $0.89^{+0.10}_{-0.07}$ |
| $b^*(\xi_{20})$                                    | $1.26^{+0.18}_{-0.25}$  | $1.47^{+0.15}_{-0.27}$  | $1.05^{+0.22}_{-0.15}$  | $1.15^{+0.13}_{-0.16}$  | $0.89^{+0.05}_{-0.03}$  | $1.32^{+0.19}_{-0.11}$  | $0.86^{+0.09}_{-0.06}$ |
| $b(\sigma_8)$                                      | $1.23^{+0.12}_{-0.17}$  | $1.52^{+0.12}_{-0.10}$  | $1.20^{+0.10}_{-0.16}$  | $1.20^{+0.15}_{-0.12}$  | $0.96^{+0.05}_{-0.05}$  | $1.20^{+0.11}_{-0.06}$  | $0.75^{+0.06}_{-0.06}$ |
| $b^*(\sigma_8)$                                    | $1.17^{+0.11}_{-0.15}$  | $1.45^{+0.11}_{-0.08}$  | $1.14^{+0.09}_{-0.15}$  | $1.14^{+0.14}_{-0.11}$  | $0.92^{+0.04}_{-0.04}$  | $1.14^{+0.10}_{-0.05}$  | $0.71^{+0.05}_{-0.05}$ |
| $\log\left(\frac{M_{DMH}}{h^{-1}M_{\odot}}\right)$ | $12.93^{+0.22}_{-0.29}$ | $13.30^{+0.26}_{-0.44}$ | $12.88^{+0.20}_{-0.40}$ | $12.88^{+0.27}_{-0.32}$ | $12.18^{+0.18}_{-0.24}$ | $12.88^{+0.20}_{-0.14}$ | $10.46^{+0.80}$        |

**Figure 4.** The  $^{0.1}u-g$  histograms for the galaxies (solid line) and the AGN (dashed line). For clarity, the AGN histogram has been scaled, by the ratio  $N_G/N_A$ , where  $N_G$  and  $N_A$  are the number of galaxies and AGN, respectively.

In agreement with Coil et al. (2009) we also find that AGN in red hosts are more clustered than those in blue galaxies. However, they find that the difference in AGN clustering due to the host color is more apparent for their  $z \sim 1$  AGN than in our sample at  $z = 0.1$ . The relative bias between red and blue AGN at  $z \approx 1$ ,  $b_{rel} \sim 1.9$  (see Table 2 of Coil et al. 2009) compared to  $b_{rel} \sim 1.3$  at  $z \approx 0.1$  (Table 4). Similarly, our relative bias estimation for the red/blue galaxies is  $b_{rel} \sim 1.35$ . Coil et al. (2009) do not give a value for this measurement, but using their quoted relative bias values for red/blue AGN, red AGN/red galaxies and blue AGN/blue galaxies we infer a red/blue galaxy relative bias of  $b_{rel} = 2.02 \pm 0.49$  at  $z \approx 1$ . This apparent discrepancy is because of the differential evolution with redshift of the bias of dark matter halos of different masses. This is demonstrated

in Fig. 8 which shows how the relative bias of red/blue AGN and galaxies evolves with redshift.

Gilli et al. (2005) and (2009) measured the projected auto-correlation function of X-ray AGN in the Chandra Deep Field South (CDFs), Chandra Deep Field North (CDFN) and the COSMOS surveys. AGN in the CDFs have luminosities comparable to those of Coil et al. (2009), although the COSMOS sample is more X-ray luminous, because of the large angular size ( $2 \text{ deg}^2$ ) and shallower depth of the X-ray survey in that field. Gilli et al. (2005, 2009) find that sample variance has a strong effect on their results, even in the wide-angle COSMOS sample, resulting in large values for the clustering length and the corresponding dark matter halo masses,  $\log M_{DMH} \sim 13.5 h^{-1} M_{\odot}$ . Narrow peaks in the AGN redshift distribution have a significant contribution to the clustering signal and are primarily responsible for the high  $M_{DMH}$  estimates. Preferentially removing galaxies in those peaks decreases the AGN bias in the CDFs and the COSMOS to values comparable to those of Coil et al. (2009) and to our estimates. However, Marulli et al. (2009) argue that sample variance cannot account for the large clustering length in the CDFs. They use semi-analytic models to follow the cosmological evolution of AGN and produce mock AGN catalogues with selection functions similar to the CDFN and the CDFS. Although the clustering of AGN in their simulations is in good agreement with the observations in the CDFN (Gilli et al. 2005) they cannot account for the large clustering signal in the CDFS within  $2.0 - 2.5\sigma$ . These results highlight the importance of developing methods which account for sample variance (e.g. cross-correlation function, see also Allevato et al. 2011).

In addition to X-ray selected AGN, Figure 7 (crosses) and Table 5 also include measurements for the bias of UV/optically selected QSOs from Mountrichas et al. (2009), Ross et al. (2009) and Ivashchenko et al. (2010). The latter study measured the auto-correlation function of  $\sim 50,000$  SDSS quasars at  $\bar{z} = 1.47$ . We estimate that their quasar bias is  $b = 2.06 \pm 0.10$  which is higher than their calculation,  $b = 1.44 \pm 0.22$ . This discrepancy is likely because of the different methodology they follow for the bias estimation. They use the redshift-space and real-space measurements to calculate the infall parameter ( $\beta$ ; see their eqn 7) and based on this calculation they estimate the AGN bias ( $\beta = f(\Omega_m, z)/b$ ; see their section 4.1 for more details). Ross



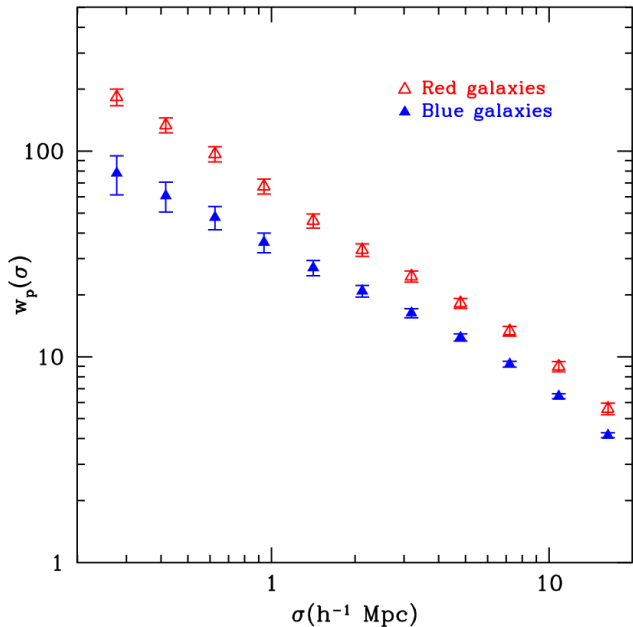


**Figure 5.** Cross-correlation functions of blue galaxies ( $^{0.1}(u-g) < 1.5$ ) with the galaxy sample (filled triangles) and red galaxies with the galaxy sample (open triangles). Red galaxies cluster more than blue galaxies.

et al. (2009) used  $\sim 30,000$  spectroscopic SDSS quasars, over the redshift range  $0.3 \leq z \leq 2.2$ . We estimate a bias for their QSOs of  $b = 2.30^{+0.15}_{-0.20}$  (Table 5). This is higher than  $b = 2.06 \pm 0.03$  that they find using a methodology similar to that of Ivashchenko et al. (2010). The discrepancy between the two numbers is likely because of the different approaches used to infer the QSO bias.

Figure 7 shows that in a redshift range  $0 < z < 2$  the AGN bias datapoints cluster around the curve that corresponds to dark matter halos with mass  $M_{\text{DMH}} \sim 10^{13} h^{-1} M_{\odot}$ . This seems to be the case for both moderate luminosity X-ray AGN and powerful UV/optical quasars as presented above. We caution however, that many optical studies (Croom et al. 2005, Myers et al. 2007, da Ángela et al. 2008) find lower masses for the dark matter halos of powerful UV bright QSO,  $M_{\text{DMH}} \sim 5 \times 10^{12} h^{-1} M_{\odot}$ . The results from those studies are not shown in Figure 7 for the reasons discussed at the beginning of the section.

## 6 COMPARISON WITH MODELS OF AGN FUELING AND EVOLUTION

This paper explores the environment of moderate luminosity X-ray AGN at  $z \approx 0.1$  by estimating their cross-correlation function with the SDSS Main Galaxy spectroscopic sample. The adopted methodology has advantages compared to auto-correlation function studies, in that random and systematic uncertainties can be better controlled. Our clustering methodology, AGN selection function and X-ray luminosity range are very similar to those of Coil et al. (2009) at  $z \approx 1$ . This allows direct comparison of the clustering properties of moderate luminosity AGN across redshift by min-

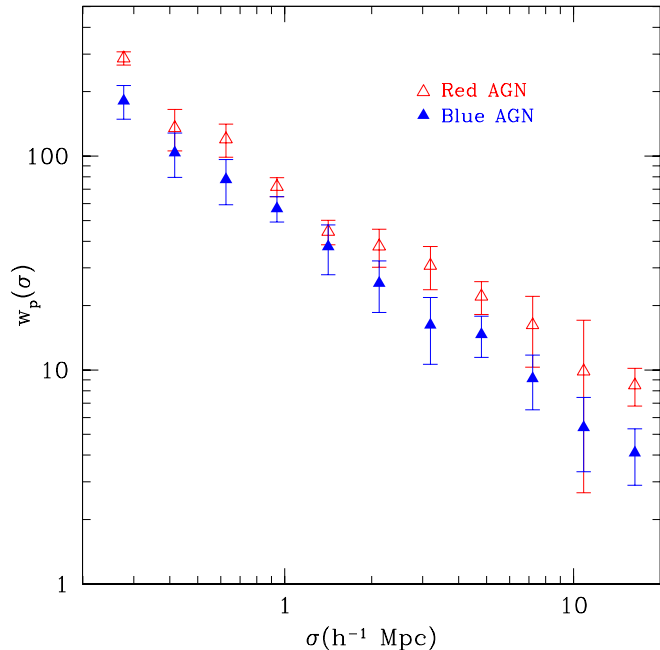


**Figure 6.** Blue ( $^{0.1}(u-g) < 1.5$ ) AGN cross-correlation function with galaxies (filled triangles) versus the red-AGN/galaxy cross-correlation function (open triangles). Red AGN cluster more than blue AGN. For clarity, open and filled triangles are offset in the horizontal direction by  $\delta \log \sigma = -0.01$  and  $+0.01$ , respectively.

imising differential selection effects. Our results combined with those of Coil et al. (2009) show that moderate luminosity X-ray selected AGN live in dark matter halos with masses  $M_{\text{DMH}} \approx 10^{13} h^{-1} M_{\odot}$  at all redshifts since  $z \approx 1$ . If powerful UV/optically selected QSOs reside in lower mass halos (few times  $10^{12} h^{-1} M_{\odot}$ ), as suggested by some studies (e.g. Croom et al. 2005, Myers et al. 2007, da Ángela et al. 2008, Ross et al. 2009, but see Figure 7), then the fueling mode of those sources may be different from that of the X-ray selected moderate luminosity AGN studied in this paper.

Semi-analytic models for the growth of SMBH that assume mergers as the main mechanism for triggering AGN activity, predict parent dark matter halos similar to those determined for UV/optically selected QSOs and lower than those estimated here for moderate luminosity X-ray AGN (e.g. Marulli et al. 2008, Bonoli et al. 2009). Thus our results argue against major mergers as the main channel for fueling the SMBH in moderate luminosity AGN. Allevato et al. (2011) have recently expanded this conclusion to higher X-ray luminosities,  $L_X \approx 10^{44} \text{ erg s}^{-1}$ . They used the XMM-COSMOS field to estimate dark matter halos in excess of  $10^{13} h^{-1} M_{\odot}$  for powerful X-ray sources. This suggests that a substantial fraction of the accretion density in the Universe is associated with dark matter haloes with masses  $\approx 10^{13} h^{-1} M_{\odot}$ , higher than what merger models predict.

Stochastic accretion as described in Hopkins & Hernquist (2006) cannot explain the massive dark matter halos of moderate luminosity AGN. In this model, disk instabilities or minor interactions fuel at high accretion rates relatively small SMBHs in spiral galaxies with abundant cold

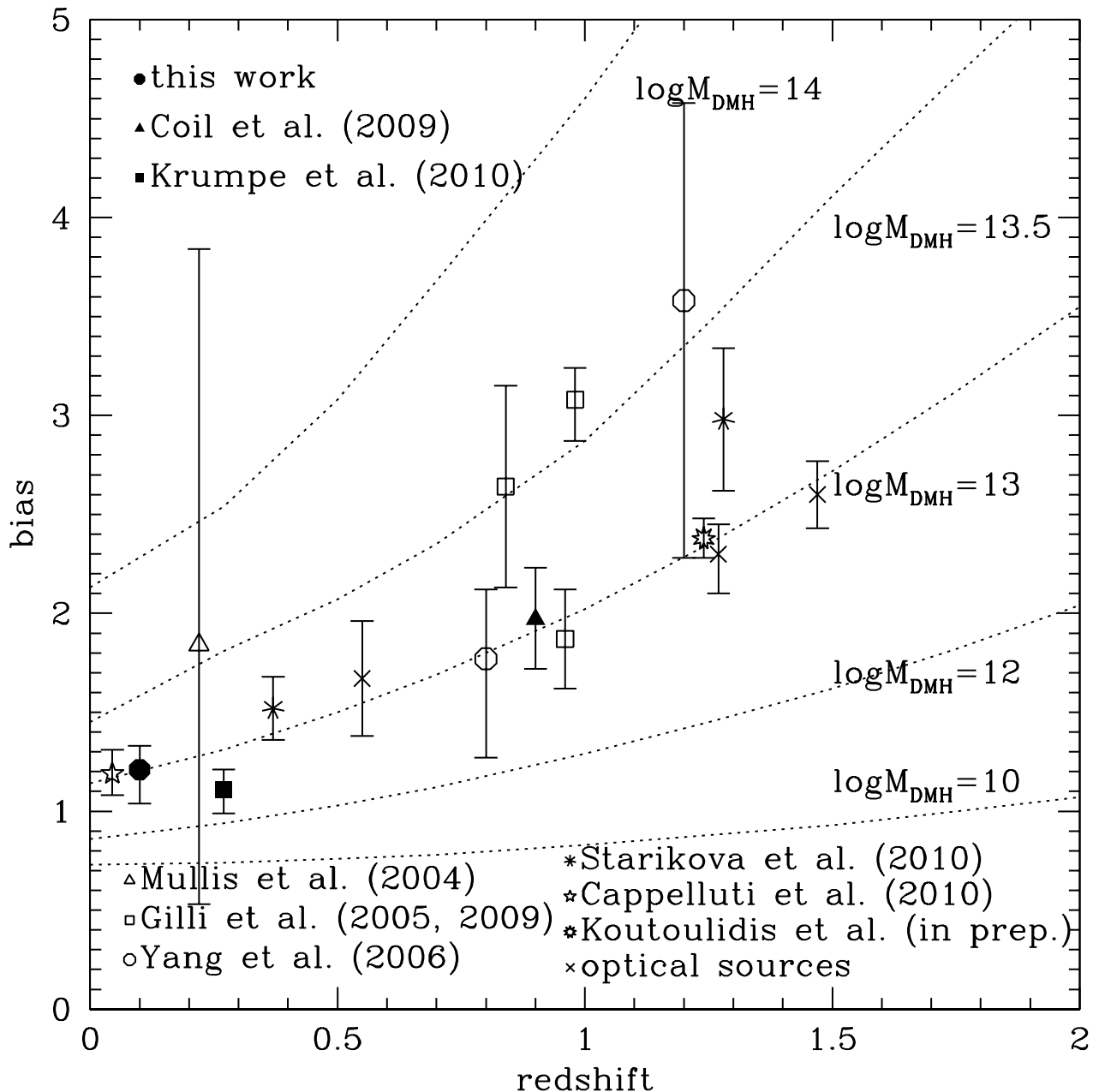


**Figure 7.** Comparison of our bias estimation (filled circle) to other studies. Crosses present the estimated biases for optical samples. From low redshift to high redshift, Mountrichas et al. (2008), Ross et al. (2009) and Ivashchenko et al. (2010). The dotted lines present the expected  $b(z)$  of dark matter halo masses. Dark matter halos have been estimated as described in the text (in units of  $h^{-1}\text{Mpc}$ ).

gas supply. This mechanism produces by design moderate luminosity AGN, which however, are predicted to lie in low density environments, as this is where large gas reservoirs, i.e. blue galaxies, are typically found, particularly at low redshift.

A more promising alternative is the model of Ciotti & Ostriker (2001), in which stellar winds from evolved stars in quiescent early type galaxies provide the fuel to supply the SMBH. The accretion energy heats the ambient gas,

slowing down subsequent infall when the Compton temperature of the emitted radiation is higher than the mean galactic gas temperature. Evolution in this case is characterized by strong oscillations, in which very fast and energetic AGN bursts are followed by longer periods during which the SMBH is dormant. This fueling mode applies to elliptical galaxies, which reside, on average, in dark matter halos similar to those of our moderate luminosity AGN sample.

One approach for getting insights into the growth of

**Table 4.** Results for the relative bias.

| Sample                   | Relative bias                |                             |
|--------------------------|------------------------------|-----------------------------|
|                          | $0.25 < \sigma < 8h^{-1}Mpc$ | $1.0 < \sigma < 8h^{-1}Mpc$ |
| AGN full/hard            | $1.05^{+0.05}_{-0.08}$       | $1.03^{+0.04}_{-0.07}$      |
| AGN red/blue             | $1.28^{+0.17}_{-0.08}$       | $1.25^{+0.15}_{-0.10}$      |
| galaxies red/blue        | $1.35^{+0.06}_{-0.06}$       | $1.29^{+0.04}_{-0.04}$      |
| red AGN/red galaxies     | $1.09^{+0.05}_{-0.03}$       | $1.07^{+0.04}_{-0.03}$      |
| blue AGN/blue galaxies   | $1.15^{+0.04}_{-0.07}$       | $1.07^{+0.05}_{-0.05}$      |
| (full) AGN/red galaxies  | $0.91^{+0.03}_{-0.06}$       | $0.95^{+0.02}_{-0.06}$      |
| (hard) AGN/red galaxies  | $0.91^{+0.04}_{-0.05}$       | $0.91^{+0.02}_{-0.06}$      |
| (full) AGN/blue galaxies | $1.37^{+0.08}_{-0.08}$       | $1.30^{+0.06}_{-0.06}$      |
| (hard) AGN/blue galaxies | $1.32^{+0.08}_{-0.08}$       | $1.25^{+0.05}_{-0.05}$      |

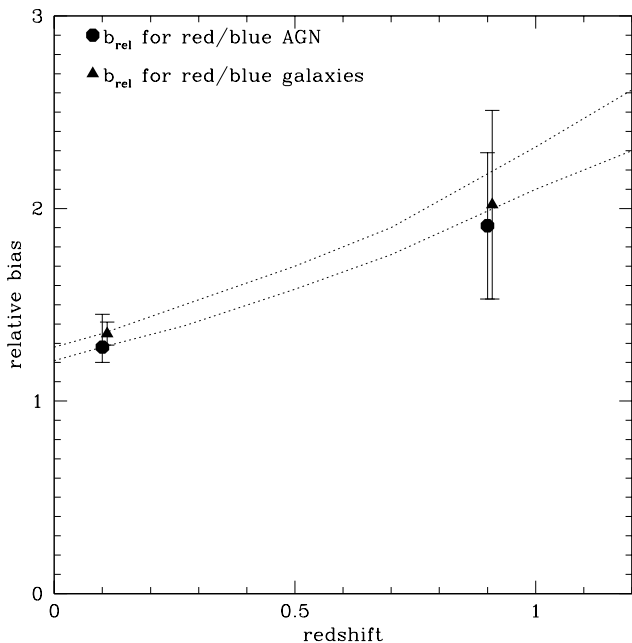


**Figure 8.** Relative bias for red/blue AGN (filled circle at  $z = 0.1$ ) and red/blue galaxies (filled triangle). Triangles are offset by 0.01 for clarity. Dotted lines show how the (relative) bias evolves with redshift. At  $z = 0.9$  the  $b_{rel}$  of Coil et al. (2009) are plotted. The higher relative bias values at  $z = 0.9$  are in agreement with those at  $z = 0.1$ , given the redshift evolution of the relative bias.

SMBH is to investigate how the baryonic matter evolves within the typical dark matter haloes that AGN are found. Empirical methods have been developed recently to connect galaxies to haloes at different epochs to constrain the history of galaxy assembly (e.g. Zheng et al. 2007, Conroy & Wechsler 2009, Zehavi et al. 2011, Avila-Reese & Firmani 2011). Although these methods cannot directly probe the formation of SMBH at the centres of galaxies, they can provide useful information on the conditions under which black holes grow.

A key result from the studies above is that the ratio of galaxy to halo mass shows a peak at the dark matter mass scale of about  $10^{12} h^{-1} M_{\odot}$ , which depends only mildly on redshift, and then decreases at higher/lower masses (e.g. Leauthaud et al. 2011, Conroy & Wechsler 2009). The halo mass where star-formation is most efficient is close to that measured for luminous UV/optically selected QSOs, which are proposed to be the products of gaseous major mergers (e.g. Di Matteo et al. 2005, Hopkins et al. 2008, Marulli et al. 2008, Bonoli et al. 2009). In contrast, moderate luminosity X-ray AGN at both  $z \approx 0.1$  and  $z \approx 1$  (e.g. Coil et al. 2009) live in haloes that are, on average, offset from the sites where star-formation proceeds more efficiently. The typical dark matter halo of these systems ( $10^{13} h^{-1} M_{\odot}$ ) corresponds to the scale where satellites start to dominate the stellar mass budget of the halo (e.g. Leauthaud et al. 2011), i.e. small and moderate size groups (e.g. Coil et al. 2004). This might indicate that moderate luminosity X-ray AGN may be fueled by the cooling of hot gas associated with the group environment (e.g. Croton et al. 2006, Bower et al. 2006). Semi-analytic models that include prescriptions for the growth of SMBHs predict that this accretion mode can produce luminosities comparable to those of the AGN sample presented here (e.g. Fanidakis et al. 2011). Alternatively, the increasing importance of satellites in the integrated stellar mass of  $10^{13} h^{-1} M_{\odot}$  haloes suggests that they may play a role in the activation of the SMBH, e.g. via tidal interactions or mergers with the central galaxy of the halo. Semi-analytic models of galaxy evolution (e.g. Bower et al. 2006, De Lucia & Blaizot 2007) predict that the main route of stellar mass growth since  $z = 1$  of the central galaxies of haloes with present-day mass  $10^{13} h^{-1} M_{\odot}$  are mergers with satellites (Zehavi et al. 2011). As long as AGN are associated with the central galaxy of a halo (e.g. Starikova et al. 2010), such gravitational interactions may also be responsible for triggering accretion of material onto the central SMBH.

We caution however, that studies that connect stellar and halo masses in a phenomenological way find contradictory results on the importance of mergers in haloes with present-day mass  $10^{13} h^{-1} M_{\odot}$ . Conroy & Wechsler (2009) argue that in such haloes star-formation is primarily responsible for the growth of the stellar mass of the central galaxies

**Table 5.** Clustering measurements for X-ray and UV bright AGN from the literature. Columns are: (1) reference to the AGN sample. A star marks UV/optical selected QSOs; (2) methodology used to determine the clustering, i.e. auto-correlation or cross-correlation; (3) name of the survey that the AGN sample was selected from; (4) number of sources used; (5) scales used each study to determine the clustering amplitude and slope; (6) best-fit clustering amplitude measured in each study; (7) best-fit clustering slope measured in each study; (8) mean redshift of the sample; (9) the bias values re-calculated using the  $\sigma_8$  methodology discussed in the text.

| Study                         | Methodology | Sample                     | no<br>of objects | scales<br>( $h^{-1}\text{Mpc}$ ) | $r_0$<br>( $h^{-1}\text{Mpc}$ ) | $\gamma$               | $z$   | $b(\sigma_8)$          |
|-------------------------------|-------------|----------------------------|------------------|----------------------------------|---------------------------------|------------------------|-------|------------------------|
| (1)                           | (2)         | (3)                        | (4)              | (5)                              | (6)                             | (7)                    | (8)   | (9)                    |
| This Work (full)              | cross-cor   | XMM/SDSS                   | 297              | 0.25 – 17                        | $5.0 \pm 0.5$                   | $2.00 \pm 0.11$        | 0.10  | $1.23^{+0.12}_{-0.17}$ |
| This Work (hard)              | cross-cor   | XMM/SDSS                   | 175              | 0.25 – 17                        | $4.8 \pm 0.6$                   | $2.02 \pm 0.18$        | 0.10  | $1.20^{+0.15}_{-0.12}$ |
| Coil et al. (2009)            | cross-cor   | AEGIS                      | 113              | 0.1 – 8                          | $5.95 \pm 0.90$                 | $1.66 \pm 0.22$        | 0.90  | $1.97^{+0.26}_{-0.25}$ |
| Krumpe et al. (2010)          | cross-cor   | RASS                       | 1552             | 0.3 – 15                         | $4.28^{+0.44}_{-0.54}$          | $1.67^{+0.13}_{-0.12}$ | 0.27  | $1.11^{+0.10}_{-0.12}$ |
| Mullis et al. (2004)          | auto-cor    | NEP                        | 219              | 5.0 – 60                         | $7.5^{+2.7}_{-4.2}$             | $1.85^{+1.90}_{-0.80}$ | 0.22  | $1.84^{+2.00}_{-1.31}$ |
| Gilli et al. (2005)           | auto-cor    | CDFS                       | 97               | 0.2 – 10                         | $10.3 \pm 1.7$                  | $1.33 \pm 0.14$        | 0.84  | $2.64 \pm 0.51$        |
| Gilli et al. (2005)           | auto-cor    | CFDN                       | 160              | 0.2 – 10                         | $5.5 \pm 0.6$                   | $1.50 \pm 0.12$        | 0.96  | $1.87 \pm 0.25$        |
| Gilli et al. (2009)           | auto-cor    | COSMOS                     | 538              | 0.3 – 40                         | $8.65^{+0.41}_{-0.48}$          | $1.88^{+0.06}_{-0.07}$ | 0.98  | $3.08^{+0.16}_{-0.21}$ |
| Yang et al. (2006)            | auto-cor    | CFDN                       | 252              | 0.2 – 15                         | $5.8^{+1.0}_{-1.5}$             | $1.38^{+0.12}_{-0.14}$ | 0.8   | $1.77^{+0.35}_{-0.50}$ |
| Yang et al. (2006)            | auto-cor    | CLASXS                     | 233              | 1.0 – 30                         | $8.1^{+1.2}_{-2.2}$             | $2.1 \pm 0.5$          | 1.2   | $3.58^{+1.00}_{-1.30}$ |
| Starikova et al. (2010)       | auto-cor    | Bootes                     | 1282             | 0.5 – 20                         | $5.4 \pm 0.5$                   | $1.97 \pm 0.09$        | 0.37  | $1.52 \pm 0.16$        |
| Starikova et al. (2010)       | auto-cor    | Bootes                     | 1282             | 0.5 – 20                         | $7.0 \pm 0.8$                   | $1.97 \pm 0.09$        | 1.28  | $2.98 \pm 0.36$        |
| Cappelluti et al. (2010)      | auto-cor    | BAT                        | 199              | 0.2 – 200                        | $5.56^{+0.49}_{-0.43}$          | $1.64^{+0.08}_{-0.07}$ | 0.045 | $1.19^{+0.12}_{-0.11}$ |
| Koutoulidis et al. (in prep.) | auto-cor    | CDFs/ECDFs<br>COSMOS/AEGIS | 1492             | 0.2 – 20                         | $6.1 \pm 0.2$                   | 1.8 (fixed)            | 1.24  | $2.4 \pm 0.1$          |
| Mountrichas et al. (2008)*    | cross-cor   | 2SLAQ                      | 694              | 5.0 – 25.0                       | $6.7 \pm 0.6$                   | $1.75 \pm 0.10$        | 0.55  | $1.67 \pm 0.29$        |
| Ross et al. (2009)*           | auto-cor    | SDSS                       | 30,239           | 1.0 – 25.0                       | $5.45^{+0.35}_{-0.45}$          | $1.90^{+0.04}_{-0.03}$ | 1.27  | $2.30^{+0.15}_{-0.20}$ |
| Ivashchenko et al. (2010)*    | auto-cor    | SDSS                       | 52,303           | 1.0 – 35                         | $5.85 \pm 0.33$                 | $1.87 \pm 0.07$        | 1.47  | $2.60 \pm 0.17$        |

since  $z \approx 1$ . In contrast, Zheng et al. (2007) find that mergers with smaller galaxies, either satellites or central galaxies of smaller haloes, drive the stellar mass assembly since  $z \approx 1$  in those haloes, in qualitative agreement with SAMs (Zehavi et al. 2011). The discrepancy is likely related to the way galaxies are associated with dark matter haloes in different studies and the assumptions adopted to determine the contributions of star-formation and merging to the stellar mass assembly.

A limitation of schemes that connect galaxies to dark matter haloes is that they describe the average stellar mass growth as a function of both galaxy and halo mass. There is however, evidence that moderate luminosity AGN hosts are different from the typical galaxy that lives in haloes similar to those of AGN. Using the results of Behroozi et al. (2010, their Table 3) we find that dark matter haloes with masses of  $\approx 10^{13} h^{-1} M_\odot$  at  $z = 0.1$  and  $z = 1$  are predicted to have central galaxies with mean stellar masses of about  $5 \times 10^{10} h^{-2} M_\odot$  and  $6 \times 10^{10} h^{-2} M_\odot$ , respectively. The scatter in stellar mass at a fixed halo mass is about 0.16 dex (Behroozi et al. 2010). Moderate luminosity X-ray AGN hosts however, have a broad stellar mass distribution (e.g. Shi et al. 2008, Bundy et al. 2008, Georgakakis et al. 2011). Using the stellar mass function of X-ray AGN from

Georgakakis et al. (2011) for example, we estimate mean stellar masses of about  $1.5 \times 10^{10} h^{-2} M_\odot$  at  $z \approx 0.1$  and  $2 \times 10^{10} h^{-2} M_\odot$  at  $z \approx 0.8$  with a variance of about 0.4 dex at both redshifts. This indicates that X-ray AGN, for their dark matter haloes, live in smaller than average galaxies in terms of stellar mass. X-ray AGN hosts have therefore experienced less merging and/or less star-formation (possibly due to feedback processes associated with the central engine) compared to typical galaxies in dark matter haloes of similar mass. Alternatively, this might be interpreted as evidence that a fraction of the X-ray AGN are not associated with the central galaxies of their haloes but with satellites, which are expected to have a much wider stellar mass function (e.g. Leauthaud et al. 2011). Recent studies on the Halo Occupation Distribution of AGN suggest that at least some of them live in satellite galaxies (e.g. Padmanabhan et al. 2009, Miyaji et al. 2011). Contrary to that, Starikova et al. (2010) find that X-ray AGN reside close to the centres of their dark matter haloes and tend to avoid satellites.

Evidence that X-ray AGN are in lower mass galaxies for their dark matter haloes already exists in the literature. Coil et al. (2009) find that galaxies hosting X-ray AGN are more likely to reside in more massive dark matter halos than the overall galaxy population of the same color and optical

luminosity. Digby North et al. (2011) also found that X-ray AGN live on average in higher density environments compared to stellar-mass matched galaxy samples.

## 7 CONCLUSIONS

The XMM/SDSS survey is used to constrain the clustering of moderate luminosity ( $L_X(2 - 10 \text{ keV}) = 10^{41} - 10^{44} \text{ erg s}^{-1}$ ) X-ray selected AGN at  $z \approx 0.1$ . These sources are found to reside in haloes with mass of about  $\approx 10^{13} h^{-1} M_\odot$ . Comparison with studies at higher redshift, suggest that this halo mass scale corresponds to the typical environment of X-ray AGN in the luminosity interval above at least out to  $z \approx 1$ .

Haloes with masses  $\approx 10^{13} h^{-1} M_\odot$  correspond to the group scale, where satellites dominated the stellar mass budget of the halo. This suggests that either accretion of hot gas associated with the group environment or interactions of the central galaxy with satellites are responsible for the activation of the SMBH in our AGN sample.

Splitting the AGN sample by colours shows that those with red colours are more clustered than those in blue colours. This is in agreement with results at higher redshift,  $z \approx 1$ . We do not find a dependence of clustering on obscuration or accretion luminosity. A wider luminosity baseline than that spanned by our sample is probably needed to explore trends of the AGN clustering with  $L_X$ .

There is also evidence that the hosts of moderate luminosity X-ray AGN have lower stellar masses compared to the typical galaxy in haloes of the same size. This may have important implications for understanding the conditions under which supermassive black holes at the centres of galaxies grow.

## 8 ACKNOWLEDGMENTS

The authors acknowledge financial support from the Marie-Curie Reintegration Grant PERG03-GA-2008-230644. Funding for the Sloan Digital Sky Survey (SDSS) has been provided by the Alfred P. Sloan Foundation, the Participating Institutions, the National Aeronautics and Space Administration, the National Science Foundation, the U.S. Department of Energy, the Japanese Monbukagakusho, and the Max Planck Society. The SDSS Web site is <http://www.sdss.org/>. The SDSS is managed by the Astrophysical Research Consortium (ARC) for the Participating Institutions. The Participating Institutions are The University of Chicago, Fermilab, the Institute for Advanced Study, the Japan Participation Group, The Johns Hopkins University, Los Alamos National Laboratory, the Max-Planck-Institute for Astronomy (MPIA), the Max-Planck-Institute for Astrophysics (MPA), New Mexico State University, University of Pittsburgh, Princeton University, the United States Naval Observatory, and the University of Washington.

## References

Abazajian K. N., et al., 2009, ApJS, 182, 543

- Aird J., et al., 2010, MNRAS, 401, 2531  
 Akylas A., Georgantopoulos I., Plionis M., 2000, MNRAS, 318, 1036  
 Allevato et al., 2011, ApJ accepted, preprint (astro-ph/1105.0520)  
 Avila-Reese V., Firmani C., 2011, RevMexAA, (astro-ph/1103.4329)  
 Barger A. J. et al., 2003, ApJ, 584, 61  
 Basilakos S., Georgakakis A., Plionis M., Georgantopoulos I., 2004, ApJ, 607, L79  
 Basilakos S., Plionis M., Georgakakis A., Georgantopoulos I., 2005, MNRAS, 356, 183  
 Behroozi P. S., Conroy C., Wechsler R. H., 2010, ApJ, 717, 379  
 Blanton M. R., Roweis S., 2007, AJ, 133, 734  
 Blanton M. R., 2006, ApJ, 648, 268  
 Blanton M. R., et al., 2005, AJ, 129, 2562  
 Bonoli S., et al., 2009, MNRAS, 396, 423  
 Bower R., et al., 2006, ApJ, 648, 127  
 Brusa M., et al., 2009, ApJ, 693, 8  
 Bundy K., et al., 2008, ApJ, 681, 931  
 Cannon R., et al., 2006, MNRAS, 372, 425  
 Cappelluti N., et al., 2010, ApJ, 716, 209  
 Ciotti L., Ostriker J. P., 2007, ApJ, 665, 1038  
 Coil A.L., et al., 2007, ApJ, 654, 115  
 Coil A.L., et al., 2008, ApJ, 672, 153  
 Coil A.L., et al., 2009, ApJ, 701, 1484  
 Conroy C. & Wechsler R. H., 2009, ApJ, 696, 620  
 Croom S. M., et al., 2004, MNRAS, 349, 1397  
 Croom S. M., et al., 2005, MNRAS, 356, 415  
 Croom S. M., et al., 2009, MNRAS, 392, 19  
 Croton D. J., et al., 2006, MNRAS, 365, 11  
 da Ângela J., et al., 2008, MNRAS, 383, 565  
 Degraf C., Di Matteo T., Springel V., 2010, MNRAS, 402, 1927  
 De Lucia G. & Blaizot J., 2007, MNRAS, 375, 2  
 Di Matteo T., Springel V., Hernquist L., Nature, 433, 604  
 Ebrero J., Mateos S., Stewart G. C., Carrera F. J., Watson M. G., 2009, A&A, 500, 749  
 Fanidakis N., 2010, Ph.D. Thesis, Durham University  
 Fanidakis N., et al., 2011, MNRAS, 410, 53  
 Ferrarese L. & Merritt D., 2000, ApJ, 539, 9  
 Gebhardt K. et al., 2000, ApJ, 543, 5  
 Georgakakis A., et al., 2008, MNRAS, 391, 183  
 Georgakakis A., et al., 2009, MNRAS, 397, 623  
 Georgakakis A. & Nandra K., 2011, MNRAS, 414, 992  
 Georgakakis A. et al., 2011, MNRAS in press, arxiv1109.0287  
 Gilli R., et al. 2005, A&A, 430, 811  
 Gilli R., et al. 2009, A&A, 494, 33  
 Hickox R.C., et al., 2009, ApJ, 696, 891  
 Hickox R.C., et al., 2011, ApJ, 731, 117  
 Hopkins P. F., Hernquist, L., 2006, ApJS, 166, 1  
 Hopkins P. F., et al., 2007, ApJ, 662, 110  
 Hopkins P. F., Hernquist L., Cox T. J., Kere D., 2008, ApJS, 175, 356  
 Ivashchenko G., Zhdanov V. I., Tugay, A. V., 2010, MNRAS, 409, 1691  
 Kenter A., 2005, ApJS, 161, 9  
 King A., 2005, ApJ, 635, 121  
 Kormendy J. & Richstone D., 1995, ARA&A, 33, 581  
 Krumpal M., Miyaji T., Coil A. L., 2010, ApJ, 713, 558

- Leauthaud A., et al., 2011, ApJ accepted, preprint (astro-ph/1103.2077)
- Leauthaud A., et al., 2011, ApJ submitted, preprint (astro-ph/1104.0928)
- Limber D. N., 1953, ApJ, 117, 134
- Madgwick D. S., et al., 2003, MNRAS, 344, 847
- Marulli F., Crociani D., Volonteri M., Branchini E., Moscardini L., 2006, MNRAS, 368, 1269
- Marulli F., Bonoli S., Branchini E., Moscardini L., Springel V., 2008, MNRAS, 385, 1846
- Marulli F., et al., 2009, MNRAS, 396, 1404
- Miyaji T., et al., 2007, ApJS, 172, 396
- Miyaji T., Krumpel M., Coil A. L., Aceves H., 2011, ApJ, 726, 83
- Mo H. J., White S. D. M., 1996, MNRAS, 282, 347
- Mountrichas G., Sawangwit U., Shanks T., Croom S. M., Schneider D. P., Myers A. D., Pimbblet K., 2009, MNRAS, 394, 2050
- Mullis C. R., et al., 2004, ApJ, 617, 192
- Myers A. D., et al., 2005, MNRAS, 359, 741
- Myers A. D., et al., 2007, ApJ, 658, 85
- Myers, A. D., et al. 2007, ApJ, 658, 99
- Nandra K., Pounds K. A., 1994, MNRAS, 268, 405
- Padmanabhan, N., et al., 2008, ApJ, 674, 1217
- Padmanabhan, N., et al., 2009, MNRAS, 397, 1862
- Peebles P. J. E., 1979, MNRAS, 189, 89
- Peebles P. J. E., 1980, *The Large-scale Structure of the Universe*. Research supported by the National Science Foundation. Princeton Univ. Press, Princeton, NJ, p. 435
- Plionis M., Rovilos M., Basilakos S., Georgantopoulos I., Bauer F., 2008, ApJ, 674, 5
- Richards G. T., et al., 2002, AJ, 123, 2945
- Ross N. P., et al., 2007, MNRAS, 381, 573
- Ross N. P., et al., 2008, MNRAS, 387, 1323
- Ross N. P., et al., 2009, ApJ, 697, 1634
- Saunders W., Rowan-Robinson M., Lawrence A., 1992, MNRAS, 258, 134
- Schneider D. P., 2005, AJ, 130, 367
- Schlegel D. J., Finkbeiner D. P., Davis M., 1998, ApJ, 500, 525
- Shankar, F., Crocce M., Miralda-Escudé J., Fosalba P., Weinberg D.H., 2010, ApJ, 718, 231
- Shanks T., Croom S. M., Fine S., Ross N. P., Sawangwit U., 2011, MNRAS submitted, preprint (astro-ph/1105.2547v1)
- Sheth R. K., Mo H. J., Tormen G., 2001, MNRAS, 323, 1
- Shi Y., et al., 2008, ApJ, 688, 794
- Silk J. & Rees M. J., 1998, A&A, 331, 1
- Smith R. E., et al., 2003, MNRAS, 341, 1311
- Spergel D. N., et al., 2007, ApJS, 170, 377
- Springel V., et al., 2005, Nat, 435, 629
- Starikova S., et al., 2010, ApJ submitted, preprint (astro-ph/1010.1577)
- Strauss M. A., et al., 2002, AJ, 124, 1810
- Tueller J., et al., 2010, ApJS, 186, 378
- van den Bosch, F.C. 2002, MNRAS, 331, 98
- Yang Y., Mushotzky R. F., Barger A. J., Cowie L. L., 2006, ApJ, 645, 68
- Zehavi I., et al., 2005, ApJ, 630, 1
- Zehavi I., Patiri S., Zheng, Z., 2011, ApJ submitted, preprint (astro-ph/1104.0389)
- Zheng Z., Coil A. L., Zehavi I., 2007, ApJ, 667, 760